Tuning the acidic properties of aluminas via sol-gel synthesis: New findings on the active site of alumina-catalyzed epoxidation with hydrogen peroxide

Roberto Rinaldi [a], Fred Y. Fujiwara [a], Wolfgang Hölderich [b], Ulf Schuchardt [a,*]

[a] *Instituto de Química, Universidade Estadual de Campinas, PO Box 6154, 13084-971 Campinas-SP, Brazil*
[b] *Department of Chemical Technology and Heterogeneous Catalysis, RWTH-Aachen, Worringerweg 1, 52074 Aachen, Germany*

Abstract

This study answers several pending questions about alumina-catalyzed epoxidation with aqueous 70 wt% H_2O_2. To evaluate the effect of the water-to-aluminum tri-*sec*-butoxide molar ratio, this was systematically changed from 1 to 24. The xerogels were calcined at 450 °C and gave different γ-Al_2O_3's with distinct textural and acidic properties. A combination of ^{27}Al MAS NMR and TPD-NH_3 results of calcined aluminas allowed us to assign the type Ia Al–OH sites as the catalytic sites for epoxidation. The type Ib Al–OH sites have no function in catalytic epoxidation, because ethyl acetate poisons these sites. The strong acid sites of types IIa, IIb, and III Al–OH groups are responsible for the undesired H_2O_2 decomposition and decreased oxidant selectivity.
© 2006 Elsevier Inc. All rights reserved.

Keywords: Sol-gel alumina; Catalytic epoxidation; Hydrogen peroxide

1. Introduction

New catalysts for sustainable and environmentally benign chemical processes are mandatory for the chemical industry in the 21st century to decrease significant risks of chemical pollution to the health of humans and wildlife on a universal scale [1,2]. In this context, the sol-gel method is a very attractive alternative way to synthesize solids with well-defined structural, textural, morphological, and chemical properties that are extremely desirable for application in heterogeneous catalysis, showing higher conversions, selectivities and lifetimes. Studies of physical chemistry properties of these new catalysts can improve understanding of the molecular aspects involved in the catalysis promoted by these materials [3].

The sol-gel method is controlled by the relative rates of hydrolysis and condensation of the molecular precursors. Parameters that influence hydrolysis and condensation and that are deliberately varied for use in materials design are (i) the kind of precursor(s), (ii) the water-to-precursor molar ratio, (iii) the

kind of catalyst in the sol-gel synthesis, (iv) the kind of solvent, (v) the temperature, and (vi) the relative and absolute concentration in the precursor mixtures [4]. Recently, several papers have been published showing the applicability of sol-gel routes for the synthesis of aluminas with special properties tailored for catalytic applications [5–10]. Shimada et al. [11] have shown that the hydrolysis ratio, H_2O to aluminum tri-*sec*-butoxide, is an important parameter for modifying the structural and acidic properties of sol-gel-prepared alumina powders. Their results reveal no relationship between the XRD patterns and the porosity or acidity, which strongly suggests that these properties likely arise from short-range structures and are not necessarily related to the long-range structures of the aluminas.

Our interest in transition metal-free aluminas started with a joint project with Professor Roger Sheldon (TU-Delft). Aluminas were shown to efficiently catalyze the epoxidation of various nucleophilic alkenes, including terpenes [12,13] and linear, cyclic, and functionalized olefins [12,14], using aqueous 70 wt% hydrogen peroxide or anhydrous 24 wt% hydrogen peroxide in ethyl acetate. Among the advantages of using alumina as an epoxidation catalyst is that it is a nonpolluting material and that it permits the use of the environmen-

tally friendly oxidant hydrogen peroxide [15]. The γ-Al_2O_3 obtained by the calcination of precursors synthesized by different sol-gel routes showed different catalytic activities in the epoxidation of cyclohexene and (S)-limonene using anhydrous H_2O_2 in ethyl acetate. The γ-Al_2O_3 prepared from aluminum *sec*-butoxide, using oxalic acid as a gelation catalyst, showed a significantly higher epoxidation activity than commercial alumina [16]; however, different types of commercial chromatographic aluminas (acidic, neutral, and basic) had similar catalytic behaviors in the epoxidation of α-pinene [12]. In recent studies [17,18], we discovered that surface hydrophilicity plays a pivotal role in the catalytic activity of γ-Al_2O_3 and that the key factor responsible for the similar catalytic behavior of commercial chromatographic aluminas is a similar hydrophilicity [18]. However, it was not possible to distinguish what type of Al–OH surface site is responsible for epoxidation, besides a rough indication that the weak to moderate Brønsted acid sites could be the active sites for the alumina-catalyzed epoxidation, because they could be easily replaced on the alumina surface by hydrogen peroxide because of their high mobility [19,20], creating hydroperoxy groups on the surface that, due to the polarizing effect of the Al(III) ions, can activate the O–O bond, facilitating distal oxygen transfer to the nucleophilic olefin [17].

In this work, we synthesized several γ-Al_2O_3 by the calcination at 450 °C of xerogels prepared using H_2O to aluminum tri-*sec*-butoxide molar ratios of 1–24 at room temperature. The correlation of the acidic properties of these γ-Al_2O_3 with the catalytic activity for *cis*-cyclooctene epoxidation with aqueous 70 wt% H_2O_2 provided new insights into the nature of the acid sites related to catalytic epoxidation and the accompanying undesired H_2O_2 decomposition.

2. Experimental

2.1. Catalyst synthesis

The precursors were obtained by the hydrolysis of aluminum *sec*-butoxide (Merck, 99.8%). In 125-mL round-bottomed flasks, different amounts of ultrapure water (Milli-Q) were added under vigorous stirring to 50.00 g of 50 wt% aluminum *sec*-butoxide in *sec*-butanol (Merck, p.a.) to reach H_2O to Al molar ratios of 1, 2, 3, 4, 5, 6, 8, 12, and 24. (Caution: This reaction is highly exothermic.) After vigorous stirring for 5 min, the mixtures transformed into gelatinous slurries and were aged under stirring for 24 h. These gels were placed into rectangular glass plates (17 × 28 cm) and dried at room temperature for 24 h, producing the xerogels. About 3.0–4.0 g of the xerogels was calcined under a static air atmosphere at 100, 200, 300, and finally 450 °C. Thus, the xerogels were heated at 1 °C min^{-1} until each temperature level was reached, which was maintained for 3 h. For the final heating step at 450 °C, the temperature was maintained for 24 h, giving the aluminas herein denoted as A450-*x*, where *x* is the H_2O-to-Al molar ratio used in the xerogel synthesis. The calcined aluminas were then stored in closed flasks in a desiccator over silica gel and a 3 Å molecular sieve for subsequent characterization and use in epoxidation reactions.

2.2. Catalyst characterization

2.2.1. X-ray power diffraction

Powder X-ray diffraction (XRD) patterns were determined with a Shimadzu XD-3A diffractometer, using Cu$K\alpha$ radiation and 2θ from 5° to 100°, with a step size of 0.02° and a counting time of 3 s. The phase identification was done using the program PCPDFWIN v. 2.0 and the crystallographic pattern files [21-1307] and [47-1308] for boehmite and γ-Al_2O_3, respectively.

2.2.2. Surface area analysis

The nitrogen adsorption–desorption isotherms of the calcined aluminas A450-1 to A450-24 samples were measured on a Micrometrics ASAP 2010 device. The samples were degassed at 120 °C under vacuum (1 µbar) for 3 h. The surface area was determined by adsorption–desorption of nitrogen at 77 K. The pore volume and average pore diameter were calculated using the BET method.

2.2.3. Thermogravimetric analysis

Thermogravimetric analysis (TGA) of the calcined aluminas A450-1 to A450-24 was carried out under an oxidative atmosphere (synthetic air, 100 mL) using a TA Micrometrics 2950 TGA instrument with a heating rate of 20 °C in the range of 30–900 °C. The analyses were performed in duplicate for each sample.

2.2.4. Elemental analysis

Elemental analyses were carried out using a Perkin-Elmer Series II CHN S/O Analyzer model 2400. Calcined alumina samples (A450-1 to A450-24) were mixed with an oxidant mixture (Pb_3O_4:NaF, 1:7), and the elemental analyses were performed by combusting the samples at 925 °C. The analyses were done in triplicate.

2.2.5. Temperature-programmed desorption of ammonia

Temperature-programmed desorption of ammonia curves (TPD-NH_3) of the calcined aluminas A450-1 to A450-24 were measured on a TPDRO Thermo Finnigan model 1100 device. Before analysis, the samples (200.0 mg) were pretreated in situ at 300 °C for 1 h under a nitrogen flow (20 mL min^{-1}). The ammonia adsorption (3%, v/v, 20 mL min^{-1}) was done at 100 °C for 1 h. The ammonia excess was removed with a nitrogen flow (20 mL min^{-1}) at 120 °C for 3 h. The sample was cooled to 25 °C and kept under a helium flow (25 mL min^{-1}) until a constant baseline for the signal of the thermal conductivity detector (TCD) was obtained. The TPD-NH_3 analyses were started by heating the sample from 25 to 800 °C under a helium flow (25 mL min^{-1}). The flow of desorbed gas was passed through a trap containing a fresh mixture of CaO/NaOH (Natron) to remove any water or carbon dioxide traces evolved at higher temperatures. The amount of desorbed ammonia was estimated by the TCD response, previously calibrated with ammonia.

2.2.6. ^{27}Al NMR spectra

The ^{27}Al NMR spectra were recorded for the calcined aluminas A450-1 to A450-24 using a Varian INOVA 500 spectrometer, operating at 130.26 MHz and equipped with a 4-mm high-speed probe (Doty Scientific) at a spinning rate of 13 kHz. The ^{27}Al chemical shifts are referenced to a 1.0 mol L^{-1} Al(NO$_3$)$_3$ solution. The experimental conditions were acquisition time of 5 ms, pulse width of 2.4 μs ($\pi/2$), recycle delay of 0.1 s, and spectral width of 32.2 kHz. For each spectrum, 2400 scans were acquired. The FIDs were processed using an exponential function with a line width of 1 Hz. The spectra were fitted using the VNMR program v. 6.2 (Varian).

2.3. Catalytic reactions

The aqueous solution of hydrogen peroxide (70 wt%) was supplied by Peróxidos do Brasil S.A. (Solvay) and used without further treatment. The reaction mixture was prepared to contain 1.00 mol L^{-1} of *cis*-cyclooctene (Acros; 95%) and 0.500 mol L^{-1} of *n*-butylether (internal standard; Acros; >99%) in ethyl acetate (Merck; p.a.).

In a two-necked round-bottomed flask were added 20.00 mL of the reaction mixture (20.0 mmol of cyclooctene and 10.0 mmol of *n*-butylether) and 2.00 mL (56 mmol) of aqueous 70 wt% H$_2$O$_2$. The mass of the reaction mixture was determined for calculation of the hydrogen peroxide content. This mixture was heated to 80 °C with magnetic stirring. An initial aliquot ($t = 0$ h) was taken for gas chromatography (GC) analysis, and the reaction was started by addition of the alumina (200.0 mg). Aliquots (50 μL) were taken at 1, 3, 6, 12, and 24 h; diluted in hexane (2 mL; Tedia; HPLC-grade); and treated with a few milligrams of manganese dioxide to promote decomposition of the peroxides and then with anhydrous sodium sulfate to remove residual water. These solutions were analyzed using a Hewlett–Packard HP 5890 Series II gas chromatograph equipped with an Alltech AT-WAX capillary column (20 m × 0.25 mm × 0.25 μm film thickness) and a flame ionization detector. The *cis*-cyclooctene epoxide was quantified using a calibration curve obtained with a standard solution. Selectivity is always given with respect to converted *cis*-cyclooctene.

2.4. Determination of hydrogen peroxide

Into an Erlenmeyer flask were added 50 mL of aqueous 20 wt% acetic acid and 20 g of dry ice to deaerate the solution. After 2 min, ca. 2.0 g of potassium iodide (Synth; p.a.) and 3 drops of a 1 wt% ammonium molybdate solution (Vetec; p.a.) were added. To this mixture, 200-mg aliquots of the reaction mixture, collected at 0, 1, 3, 6, 12, and 24 h, were added. The iodine formed was titrated with a 0.1000-mol L^{-1} solution of sodium thiosulfate (Synth; p.a.). Near the endpoint of the titration (pale brown color), 1.0 mL of a 1-wt% starch solution was added. The endpoint was detected when the blue color disappeared. The amount of H$_2$O$_2$, in mmol, in the reaction mixture was calculated by

$$n_{H_2O_2} = \frac{C_{S_2O_3^{2-}} \cdot V_{S_2O_3^{2-}}}{2} \cdot \frac{m_{reaction}}{m_{aliquot}} \times 10^3, \tag{1}$$

where $C_{S_2O_3^{2-}}$ is the concentration of the sodium thiosulfate solution (mol L^{-1}), $V_{S_2O_3^{2-}}$ is the volume of sodium thiosulfate solution (L), $m_{reaction}$ is the mass of the reaction mixture (g), and $m_{aliquot}$ is the mass of the aliquot (g) taken after 0, 1, 3, 6, 12, and 24 h. To determine the H$_2$O$_2$ content at 1, 3, 6, 12, and 24 h, the alumina mass was included in the mass of the reaction mixture.

3. Results and discussion

In previous reports [16,18,21], oxalic acid was used in the sol-gel syntheses to obtain nanocrystalline boehmite xerogels. Oxalic acid acts as a moderator of hydrolysis and polycondensation reactions of the molecular precursors in sol-gel syntheses [3,4], creating the framework of aluminum (oxy-)hydroxides, as the oxalate anions can coordinate to the Al(III) ions. In this work, we did not use oxalic acid in the sol-gel synthesis of the precursors, because it could disguise the H$_2$O-to-Al molar ratio effect on the properties of calcined aluminas. The xerogels synthesized with H$_2$O-to-Al ratios <3 (substoichiometric water amount) were predominately amorphous; $3 \leqslant$ H$_2$O to Al < 8 ratios gave a boehmite structure; and for H$_2$O to Al $\geqslant$ 12 ratios, the xerogels crystallize as a mixture of boehmite [γ-AlOOH] and bayerite [β-Al(OH)$_3$]. After calcination at 450 °C, the xerogels lose their structures and were transformed into γ-Al$_2$O$_3$. Table 1 summarizes the textural and structural properties of the calcined aluminas A450-1 to A450-24.

In the catalytic epoxidation of *cis*-cyclooctene with aqueous 70 wt% H$_2$O$_2$, using the activated aluminas prepared by calcination at 450 °C of the xerogels synthesized with different H$_2$O to Al molar ratios, Fig. 1 shows that the aluminas A450-5 and A450-6 gave higher yields of cyclooctene oxide (around 70% after 24 h). The selectivity for epoxide after 24 h was in the range of 95–98% for all calcined aluminas, with exception of A450-1, which showed the lowest selectivity, around 90%. Based on the average H$_2$O$_2$ consumption per epoxide formed (oxidant efficiency), the aluminas A450-5 and A450-6 were also more efficient (Fig. 2). The H$_2$O$_2$ efficiency for aluminas A450-5 and A450-6 was around 3 mmol of oxidant per mmol of epoxide formed. The reaction without catalyst yielded around 2 mmol of epoxide (10%) after 24 h, using up 1.1 mmol of H$_2$O$_2$ per mmol of epoxide formed. Figs. 1 and 2 show that the aluminas with higher epoxide yields have also lower H$_2$O$_2$ consumptions.

With respect to the textural properties (Table 1), these aluminas confirm the results already reported [17,18] that γ-Al$_2$O$_3$ with nonstructural pores, that usually have larger pore diameters, are better for this kind of reaction. We believe that these characteristics avoid the entrapment of water in the porous system, which would make the diffusion of the olefin to active sites more difficult [18]. Furthermore, in the epoxidation of highly reactive olefins, such as terpenes, aluminas with structural pores, usually ink-bottle shaped, are less selective because the residence time inside these pores can be sufficiently long for further oxidation or ring-opening reactions, resulting in the formation of byproducts and decreasing the selectivity for epoxides [13].

Table 1
Textural and structural properties of the calcined aluminas A450-1 to A450-2

Alumina	H_2O to Al molar ratio	A_{BET} (m^2/g)	Average pore diameter (nm)	Pore volume (cm^3/g)	Pore shape	Crystalline structure
A450-1	1	197	10.7	0.53	Slits[a]	γ-Al_2O_3
A450-2	2	210	12.2	0.65		γ-Al_2O_3 + boehmite[b]
A450-3	3	265	12.6	0.85		γ-Al_2O_3
A450-4	4	332	10.6	0.88	Interconnected cylinders[a]	γ-Al_2O_3
A450-5	5	285	16.6	1.19		γ-Al_2O_3
A450-6	6	288	16.4	1.19		γ-Al_2O_3
A450-8	8	273	14.8	1.04		γ-Al_2O_3
A450-12	12	254	9.1	0.59	Ink-bottle	γ-Al_2O_3 + boehmite[b]
A450-24	24	279	4.6	0.32		γ-Al_2O_3 + boehmite

[a] Non-structural pores.
[b] Low content of boehmite.
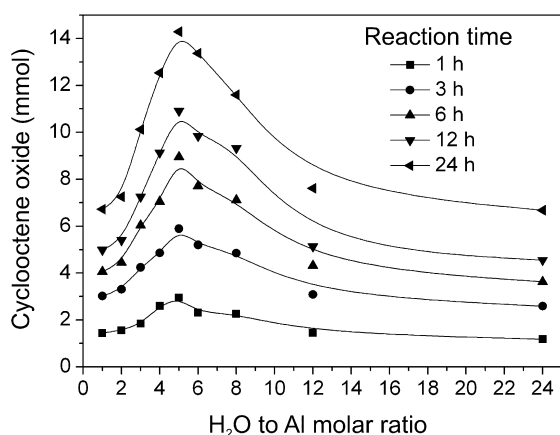
Fig. 1. Profiles of cyclooctene oxide yields at different reaction times. Catalyst: calcined aluminas A450-1 to A450-24. Reaction conditions: 20 mmol of *cis*-cyclooctene, 10 mmol of di-*n*-butylether, 56 mmol of (70 wt%) H_2O_2 and 200.0 mg of alumina; $T = 80\,°C$.
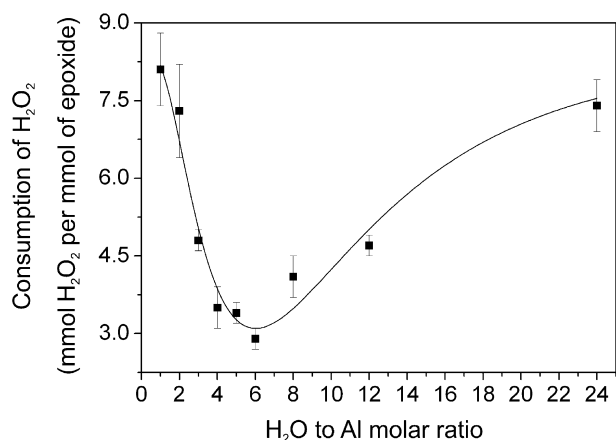

Fig. 2. Profile of average H_2O_2 consumption per mmol of epoxide formed for calcined aluminas A450-1 to A450-24. The deviation bars indicate the observed variation for aliquots taken at 1, 3, 6, 12 and 24 h.

The trends shown in Figs. 1 and 2 are quite thought-provoking, because these aluminas calcined at 450 °C have mostly γ-Al_2O_3 structure, which strongly suggests that the catalytic behaviors arise from short-range structures, that is, from the acidity and hydrophilicity of these aluminas. γ-Al_2O_3 has
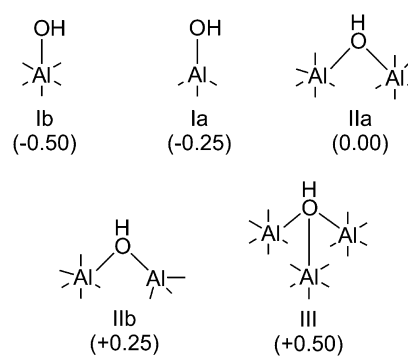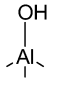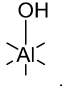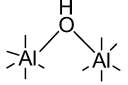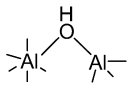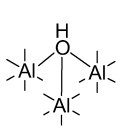

Fig. 3. Idealized hydroxyl configurations on the alumina surface proposed in the Knözinger and Ratnasamy model [24]. The values in parentheses are the global charge on the hydroxyl groups.

many types of Brønsted acid sites on the surface. Analyzing the trends of Figs. 1 and 2 from this standpoint, these results suggest that some sites are responsible for the epoxidation and others for H_2O_2 decomposition [17].

The H_2O_2 activation on the alumina surface is proposed to occur by the reaction of Brønsted acid sites, Al–OH, with H_2O_2, giving superficial hydroperoxides, Al–OOH, which are responsible for oxygen transfer to the olefin [22]. The presence of Lewis acid sites ($-O-Al^{3+}-O-$) is not expected, since the oxidant is in aqueous solution and promotes water production during the reaction. Some new insights into hydroxyls on the γ-Al_2O_3 surface have been proposed using DFT calculations [23], but no apparent contradiction with the earlier empirical Knözinger and Ratnasamy model [24] for alumina surface exists. Therefore, this empirical model is a useful tool and the easiest way to rationalize the different Al–OH groups on the surface. The Knözinger and Ratnasamy model proposes that the (111), (110), and (100) faces are covered by hydroxyl and that five configurations can be present (Fig. 3). The hydroxyls at the terminal configurations of the surface (types Ia and Ib) are the less acidic and more labile groups, whereas the hydroxyls in the bridged configurations (types IIa, IIb, and III) are sluggish and prone to act as proton donors [19,20]. According to the global charge on each hydroxyl type, the acidity order for the Al–OH groups is proposed to be Ib < Ia < IIa < IIb < III

Table 2
Idealized density of Brønsted acid sites on the γ-Al$_2$O$_3$ surface calculated from Ref. [24]

Brønsted acid site	Hydroxyl density (10^{15} cm^{-2})	Related AlO$_x$ sites (10^{15} cm^{-2})
Ia $\quad$ OH–Al	2.18	2.18 (AlO$_4$)
Ib $\quad$ OH–Al	0.83	0.83 (AlO$_6$)
IIa $\quad$ H–O(Al)(Al)	1.55	3.10 (AlO$_6$)
IIb $\quad$ H–O(Al)(Al)	1.08	1.08 (AlO$_6$)
		1.08 (AlO$_4$)
III $\quad$ H–O(Al)(Al)(Al)	0.36	1.08 (AlO$_6$)

Fig. 4. ^{27}Al MAS NMR spectra of the calcined aluminas A450-1 to A450-24.

Fig. 5. Relative population of AlO$_4$, AlO$_5$ and AlO$_6$ sites in the γ-Al$_2$O$_3$ bulk of calcined aluminas A450-1 to A450-24, estimated by fitting of the ^{27}Al MAS NMR spectra.

[24]. Using this classification, it is not easy to rationalize the large differences of acidic strength between the sites of type Ia and type III, but an estimation indicates that this difference is of the order of 10^8, considering a liquid–solid interface commonly found in aqueous suspensions of γ-Al$_2$O$_3$ [25]. The hydroxyls of type Ia and Ib are the most labile. Therefore, it is expected that at these sites the ligand exchange of –OH by –OOH should be kinetically faster. On the other hand, sites IIa, IIb, and III behave mainly as proton donors, and for this reason are likely to acid-catalyze H$_2$O$_2$ decomposition to H$_2$O and dioxygen [21]. Indeed, Lefler and Miller [26] reported that the adsorption of organic peroxides on the alumina surface creates at least two populations of superficial hydroperoxides, Al–OOH, which behave differently with respect to kinetic stability for the decomposition into dioxygen.

The Knözinger and Ratnasamy model [24] proposes an idealized γ-Al$_2$O$_3$ surface covered by hydroxyls in a perfect termination of the bulk structure in the (111), (110), and (100) faces. In this way, the population of tetrahedral (AlO$_4$) and octahedral (AlO$_6$) sites in the bulk structure can be apparently related to the several hydroxyl populations on the surface (Fig. 3). Considering the ideal values for lattice site densities on the (111), (110), and (100) γ-Al$_2$O$_3$ faces, calculated by Knözinger and Ratnasamy [24], we correlated the total density of each hydroxyl type with the equivalent number of AlO$_x$ sites in the bulk (Table 2). The configuration Ia corresponds to 66.9% of the total surface AlO$_4$ sites, and the configuration Ib corresponds to 13.6% of the total surface AlO$_6$ sites. Therefore, terminal-hydroxyls (weaker acid sites) are bonded mainly to four-coordinated Al(III) ions, and the bridged-hydroxyls (most acidic sites) are bonded mainly to six-coordinated Al(III) ions.

^{27}Al MAS NMR is a very useful tool for estimating the relative population of Al(III) ion sites in aluminas [10]. Distortions in the Al(III) coordination sphere are associated with a larger electric field gradient that may give rise to broad resonance lines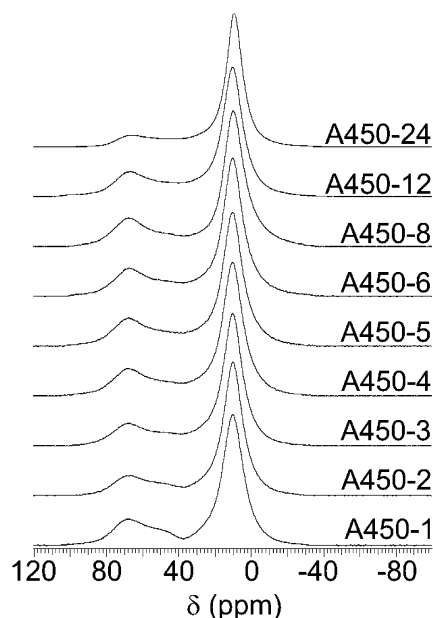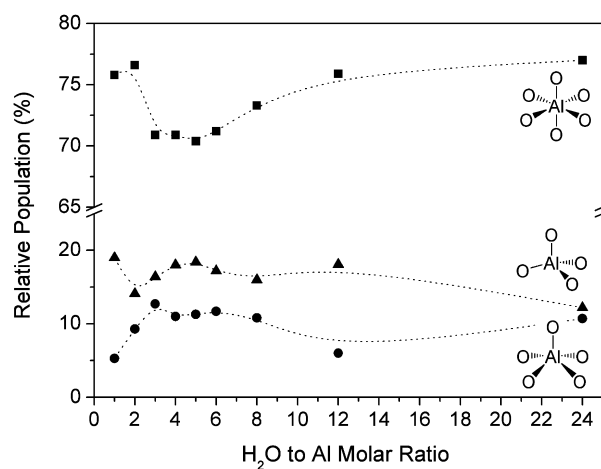 due to the quadrupolar moment of Al(III), which may make highly distorted sites invisible to ^{27}Al MAS NMR spectroscopy [27]. However, this problem is minimized using high magnetic fields, thereby taking advantage of the inverse proportionality of the second-order quadrupole interaction with the magnetic field and also of the increase in chemical shift dispersion [28]. The relative populations of AlO$_4$ ($\delta \cong 70$ ppm), AlO$_5$ ($\delta \cong 50$ ppm), and AlO$_6$ ($\delta \cong 10$ ppm) sites were estimated by fitting the ^{27}Al MAS NMR spectra of calcined aluminas A450-1 to A450-24 (Fig. 4).

Variations of the H$_2$O to Al molar ratio in the xerogel synthesis result in certain differences in the relative population of AlO$_x$ sites in the calcined aluminas at 450 °C (Fig. 5). Interestingly, the xerogels synthesized with $4 \leqslant$ H$_2$O:Al $\leqslant 6$ give, after calcination, γ-Al$_2$O$_3$ with a higher relative population of AlO$_4$ and AlO$_5$ sites (Fig. 5). The higher relative populations of AlO$_4$ sites in the aluminas A450-4 to A450-6 support the hy-
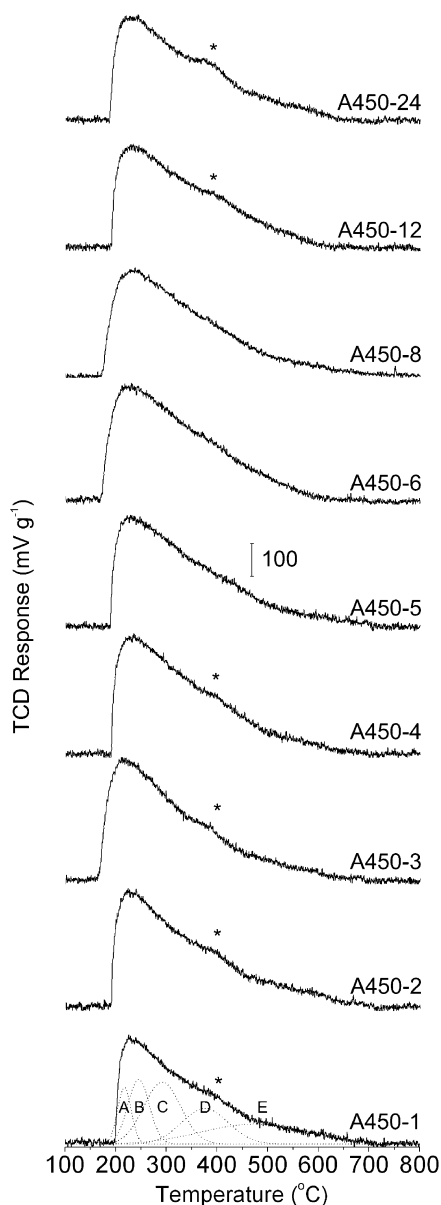
Fig. 6. TPD-NH$_3$ profiles for calcined aluminas A450-1 to A450-24. ★ indicate the "shoulder" around 400 °C assigned to strong acid sites.

pothesis that the Al–OH sites of type Ia are the active sites for epoxidation.

The strength and the amount of acid sites of aluminas was determined by temperature-programmed desorption using ammonia (TPD-NH$_3$) as the probe molecule [29,30]. The TPD-NH$_3$ profiles (Fig. 6) for calcined aluminas A450-1 to A450-24 show a broad peak indicating the existence of a wide range of acid sites on the alumina surface. However, the TPD-NH$_3$ profiles for all calcined aluminas except A450-5, A450-6, and A450-8 have a "shoulder" around 400 °C, which indicates a higher amount of strong acid sites. Therefore, the TPD-NH$_3$ profiles also support the hypothesis that the strong acid sites are responsible for H$_2$O$_2$ decomposition. To thoroughly analyze the TPD-NH$_3$ curves for calcined aluminas A450-1 to A450-24, five hypothetical curves were used to fit the experimental TPD-NH$_3$ profiles. The sum of the areas of the curves A to C

Table 3
Amount of acid sites obtained from the TPD-NH$_3$ profiles

Alumina	Amount of acid sites (μmol g^{-1})		
	Weak to moderate	Strong to very strong	Total
A450-1	76	118	193
A450-2	96	139	236
A450-3	112	128	240
A450-4	109	128	238
A450-5	138	93	231
A450-6	150	93	243
A450-8	104	115	219
A450-12	95	111	206
A450-24	95	117	212

is supposed to be related to ammonia desorption from weak to moderate acid sites and of the curves D and E to strong and very strong acid sites. The amount of acid sites calculated from the TPD-NH$_3$ curves of calcined aluminas A450-1 to A450-24 are shown in Table 3.

The trend of the quantity of weak to moderate acid sites has a behavior similar to that of yields of epoxide (Fig. 1). In contrast, the quantity of strong to very strong acid sites is related to a higher H$_2$O$_2$ consumption per mmol of formed epoxide (Fig. 2). Both trends are in agreement with the sites distribution determined by ^{27}Al MAS NMR (Fig. 5). Considering the total amount of ammonia desorbed, which represents the total amount of acid sites on the alumina surface, it is possible to estimate the quantity of type Ia and Ib sites by

$$n_{Ia} = n_{total} \times X_{AlO_4} \times 0.669 \qquad (2)$$

and

$$n_{Ib} = n_{total} \times X_{AlO_6} \times 0.136, \qquad (3)$$

where n_{Ia} and n_{Ib} are the estimated amount of Al–OH sites, in μmol g^{-1}; n_{total} is the acidity determined by TPD-NH$_3$, in μmol g^{-1}; X_{AlO_4} and X_{AlO_6} are the percentages of AlO$_4$ and AlO$_6$ present in the alumina bulk and estimated by ^{27}Al MAS NMR; and the factors 0.669 and 0.136 are, respectively, the idealized fraction of the AlO$_4$ and AlO$_6$ surface sites related to type Ia and Ib sites.

The correlation between the cyclooctene oxide productivity per m^2 versus the estimated amount of type Ia sites for the calcined aluminas A450-1 to A450-24 (Fig. 7) shows a roughly linear trend ($r^2 = 0.76$); however, no correlation between epoxide productivity and the estimated amount of type Ib sites can be observed (Fig. 8). These data reveal that the type Ia sites are strongly related to the catalytic epoxidation. The deviation observed in Fig. 8 probably arises from the dissimilarity of the pore systems (Table 1) that can make the diffusion of the olefin to active sites more difficult due to water adsorption.

We recently reported [17] that the hydrophilicity of the aluminas is a very important factor to understand alumina-catalyzed epoxidation. The surface of the calcined aluminas is rehydrated when exposed to water (from atmospheric air or from the reaction mixture). The extent of this process depends on structural and textural properties [31,32]. Thermogravimetric analyses of the aluminas, as used in the catalytic
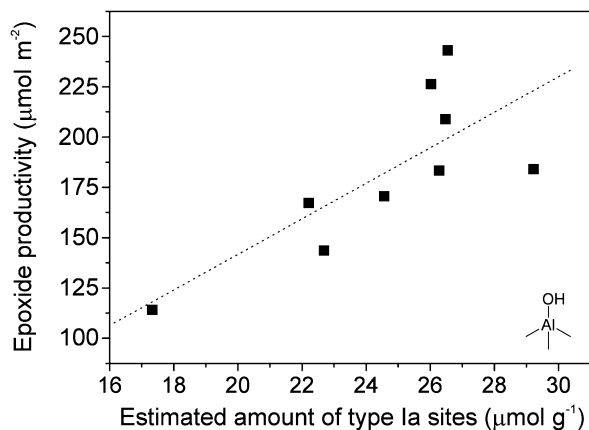
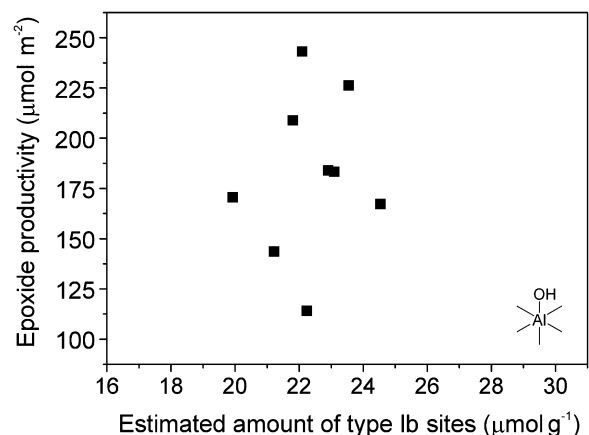Fig. 7. Epoxide productivity versus estimated amount of type Ia sites.

Fig. 8. Epoxide productivity versus estimated amount of type Ib sites.

reactions (calcined at 450 °C), were carried out to evaluate the total amount of (physically and chemically bonded) water on the alumina surfaces. (The carbon content is very low (ca. 0.3–0.6 wt%) and statistically the same for all aluminas.) The number of water molecules per nm^2 of the alumina surface can be calculated by

$$W = \frac{\Delta m}{M_{H_2O}} \cdot \frac{1}{A_{BET} \cdot m_i} \cdot N_A, \qquad (4)$$

where W is the number of water molecules per nm^2 of alumina surface at a given temperature, Δm is the weight loss (g), m_i is the initial weight of the alumina sample (g), M_{H_2O} is the molar mass of water (18.0153 g mol^{-1}), N_A is Avogadro's number (6.022 × 10^{23} mol^{-1}), and A_{BET} is the surface area determined by the BET method (nm^2 g^{-1}). To evaluate the water adsorption capacity or hydrophilicity of the calcined aluminas, we also placed these calcined aluminas into a chamber with controlled humidity and temperature for 13 days (relative humidity, 88 ± 3% and 25 ± 3 °C). After this period, the alumina were taken out and put into airtight closed flasks while awaiting thermogravimetric analysis [17]. It is important to point out that after this procedure, no powder agglomerates were formed, and the samples appeared to be homogeneous. The values of W for the original calcined samples, the values of W_{hyd} for controlled

Table 4
Number of water molecules per nm^2 of calcined aluminas, W, and of aluminas hydrated in a humidity chamber, W_{hyd}, and the ratio between these values (hydrophilicity)

Alumina	W (water molecules nm^{-2})	W_{hyd} (water molecules nm^{-2})	W_{hyd}:W ratio
A450-1	27.2 ± 0.6	50.1 ± 1.8	1.83 ± 0.04
A450-2	31.2 ± 0.2	44.2 ± 0.8	1.42 ± 0.02
A450-3	20.3 ± 1.2	32.3 ± 1.0	1.59 ± 0.07
A450-4	14.8 ± 0.2	24.6 ± 0.3	1.66 ± 0.02
A450-5	16.0 ± 0.1	25.0 ± 0.1	1.57 ± 0.01
A450-6	15.6 ± 1.4	23.6 ± 1.3	1.51 ± 0.10
A450-8	16.0 ± 1.0	23.3 ± 0.5	1.46 ± 0.07
A450-12	16.9 ± 0.1	22.4 ± 0.9	1.32 ± 0.04
A450-24	21.6 ± 0.5	23.0 ± 0.9	1.06 ± 0.05

rehydrated samples, and the W_{hyd}:W ratios (the so-called "hydrophilicity") are given in Table 4.

The calcined aluminas A450-1 to A450-24 show a narrower range of hydrophilicity (1.06–1.83) than reported earlier [17] for the aluminas calcined at 200–1000 °C (3.58–1.29). Indeed, this narrow range helped us to see some correlation between the productivity of epoxide with acidity, because short-range hydrophilic–hydrophobic interactions between the olefin and alumina surface are approximately in the same range. These interactions between the olefin and the alumina surface are complicated, because weak to moderate Brønsted acid sites (Al–OH) can act either as catalytically active sites or as inhibitors of the catalytic cycle if the surface is too highly hydroxylated, making the approach of the olefin to the alumina surface more difficult [17].

The idealized structure of γ-Al$_2$O$_3$, built up only by tetrahedral and octahedral Al(III) sites, is an approximation; many defects and distortions exist that give rise to the presence of five-coordinated (AlO$_5$) and distorted four- and six-coordinated Al(III) sites [6,23,24]. The ^{27}Al MAS NMR spectra of the calcined aluminas A450-1 to A450-24 have a resonance around 50 ppm, commonly assigned to AlO$_5$ or very distorted tetrahedral and octahedral aluminum sites [33]. Therefore, the deviation in the correlation shown in Fig. 7 is also due to distortions in the alumina structure resulting in variation of the acid strength of type Ia sites. The hydroxyls bonded on defective five-coordinated aluminum sites may also be prone to participate in the epoxidation, but it is not possible to estimate the activity of these hydroxyls in the same way as done for type Ia and Ib Al–OH groups.

Activation of H$_2$O$_2$ on alumina surfaces is believed to occur by formation of Al–OOH that, due to the polarizing effect of the Al(III) ions, activates the O–O bond, facilitating distal oxygen transfer to the olefin [13,15,17]. In fact, the O–O bond activation by alumina seems to be different compared with transition metals (Ti, Mo, W, and Re) in homogeneously catalyzed epoxidation, because these always transfer the proximal oxygen [34]. However, the proximal oxygen in Al–OOH groups on the alumina surface shows a strong steric hindrance, because the lobe of the molecular orbital σ^*_{O-O} on the proximal oxygen is directed toward the alumina surface. The correlation of epoxide productivity with type Ia sites suggests the exchange
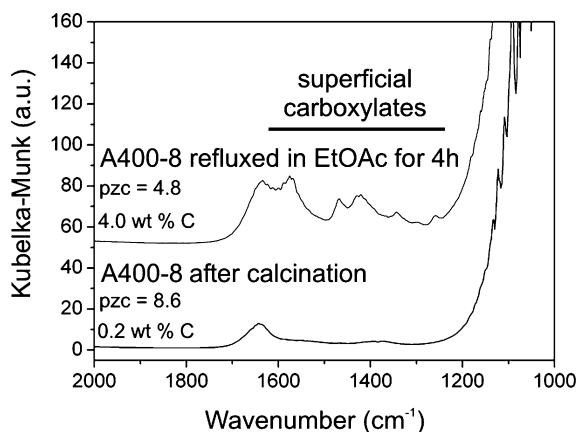
Fig. 9. FT-IR spectra for an alumina calcined at 400 °C and refluxed in ethyl acetate for 4 h.

Fig. 10. TPD-NH$_3$ analysis of calcined aluminas A450-8 and A500-8-fast-dried.

of the hydroxyls of type Ia sites with hydrogen peroxide on the alumina surface, forming superficial Al–OOH sites. The Al–O bond is predominantly ionic, meaning that polarization of the O–O bond by the Al(III) ions is due mostly to an electrostatic interaction that obeys a charge-to-size relationship with respect to the polarizing ion. In this way, Al(III) ions in a four-coordinated environment are more capable of polarizing the peroxide ligand because its ionic radius is 53 pm, much smaller than that of six-coordinated Al(III) ions (68 pm) [35]. Regarding electronic aspects, four-coordinated Al(III) sites also more efficiently polarize the O–O bond, because they are more electron-deficient than six-coordinated Al(III) sites [24]. Unfortunately, our attempts to characterize the Al–OOH groups on the alumina surface by Raman spectroscopy at room temperature, using a helium-neon laser, were not successful. In many attempts we could detect a strong line only at 876 cm^{-1}, which is assigned to $\nu_{O–O}$, normally obtained in Raman spectra of aqueous H$_2$O$_2$ solutions [36]. The lack of any other $\nu_{O–O}$ band in the range of 700–950 cm^{-1} [36], which would indicate the presence of Al–OOH, does not mean that these activated peroxide groups are not present on the alumina surface, but may indicate that they are present at too low numbers on the surface at room temperature. Indeed, alumina-supported peroxide as a reagent for epoxidation at room temperature gives low epoxide yields [22].

We have reported that basic alumina sites, such as O^{2-} or loosely bonded hydroxyls, are not able to participate in catalytic epoxidation [18,37]. This statement is in agreement with the lack of correlation shown in Fig. 8, because the hydroxyls in configuration type Ib are loosely bonded to Al(III) [24,25], which confers a basic behavior to them. We have found that using ethyl acetate is sufficient to poison type Ib Al–OH sites, because the infrared spectrum of an alumina calcined at 400 °C and refluxed in ethyl acetate usually shows several bands in the range of 1200–1600 cm^{-1}, corresponding to superficial carboxylates (Fig. 9) [38], followed by an increase in carbon content from 0.2 to 4.0% and a decrease in the isoelectric point from 8.6 to 4.8. However, no change in the catalytic performance or H$_2$O$_2$ consumption has been found [37]. Therefore, type Ib Al–OH sites do not take part in the catalytic cycle, be-
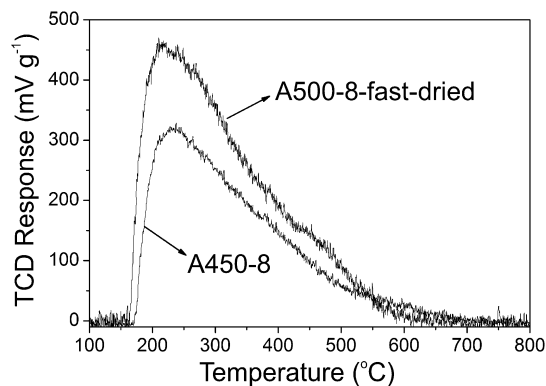
cause they are poisoned by the solvent. Indeed, several commercial chromatographic acidic and neutral aluminas are obtained by reaction of basic alumina with ethyl acetate, HCl, or acetic acid [39]. This result also explains the same catalytic behavior in α-pinene epoxidation with anhydrous H$_2$O$_2$ in ethyl acetate when using basic, neutral, weakly acidic, and acidic commercial chromatographic aluminas as catalysts [12].

We recently reported the effect of the calcination temperature on alumina-catalyzed epoxidation [17]. The precursors of these aluminas were also synthesized by the sol-gel method using a H$_2$O-to-Al molar ratio of 8; however, the gel was not aged as in the present work, but was quickly dried at 120 °C [17]. For the alumina calcined at 500 °C (A500-8-fast-dried), the epoxide yield was ca. 80% after 24 h, and consumption of H$_2$O$_2$ per mmol of cyclooctene oxide formed was 2.5 [17]. In contrast, the calcined alumina A450-8 reported here shows an epoxide yield of only 60% after 24 h and consumption of H$_2$O$_2$ per mmol of cyclooctene oxide formed was 4.1 under the same reaction conditions. To determine whether our proposed model for active sites for epoxidation and decomposition of H$_2$O$_2$ is valid, we carried out a TPD-NH$_3$ analysis for calcined alumina A500-8-fast-dried (Fig. 10).

The calcined alumina A500-8-fast-dried has a much higher amount of weak to moderate acid sites (ammonia desorption up to 300 °C). This result confirms that the weak to moderate acid sites (type Ia Al–OH groups) are the active sites for the epoxidation. However, strong acid sites (types IIa, IIb, and III Al–OH groups) are involved in the catalytic decomposition of H$_2$O$_2$, causing an undesirable decrease in oxidant selectivity. The proposed roles of each Al–OH site on the γ-Al$_2$O$_3$ surface are shown in Fig. 11.

With these insights into the role of each Al–OH site on the alumina surface in the alumina-catalyzed epoxidation, it is possible to estimate the turnover frequency and the total turnover number for the calcined aluminas synthesized in this work (Table 5). At the optimum H$_2$O to Al molar ratio in the sol-gel synthesis, the calcined alumina A450-5 shows a turnover frequency of 560 h^{-1} and a total turnover number after 24 h as high as 2690. This estimated values are similar to those of transition-metal-containing epoxidation catalysts, such as Mo(VI)/SiO$_2$ [40].
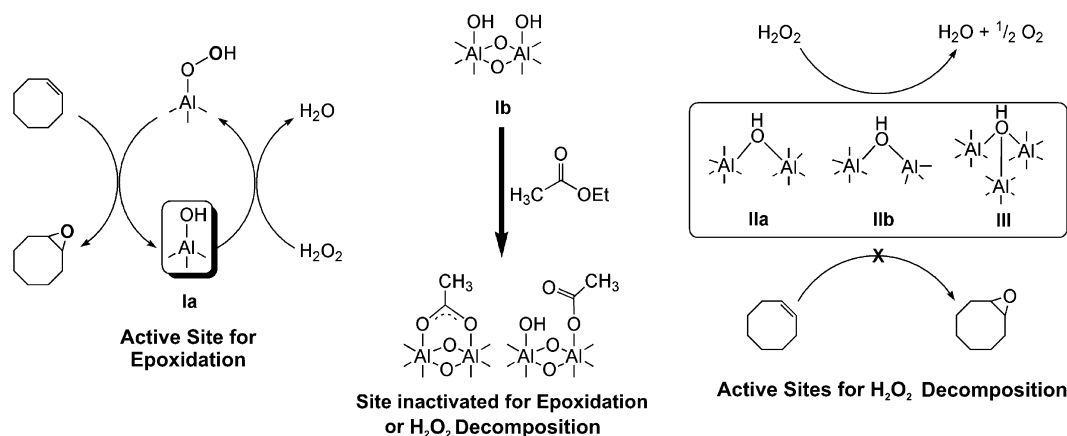
Fig. 11. Proposed role for the Al–OH sites on the alumina surface.

Table 5
Estimated turnover frequency (TOF) and total turnover number (TON) for the catalyzed epoxidation by calcined aluminas A450-1 to A450-24

Alumina	Estimated amount of type Ia acid sites ($\mu mol\,g^{-1}$)	TOF (h^{-1})	TON
A450-1	24.6	290	1370
A450-2	22.2	350	1630
A450-3	26.3	350	1930
A450-4	29.2	450	2150
A450-5	26.6	560	2690
A450-6	26.0	440	2570
A450-8	26.5	430	2190
A450-12	22.7	320	1680
A450-24	17.3	340	1930

4. Conclusions

Based on our findings, the following answers to the pending questions about alumina-catalyzed epoxidation can be stated:

1. The systematic change in the H_2O-to-Al molar ratio in sol-gel synthesis followed by calcining at $450\,^\circ C$ provided a series of γ-Al_2O_3's with distinct textural and acidic properties. The calcined aluminas A450-5 and A450-6 show higher epoxide productivity and lower consumption of H_2O_2 per epoxide formed. In previous reports, the change in the H_2O-to-Al molar ratio in sol-gel synthesis was randomized [16,18], resulting in a myriad of lower-activity catalysts but some aluminas that were very active for epoxidation. Here there is a narrow range of optimum H_2O-to-Al molar ratios in the sol-gel synthesis to produce the best-calcined alumina catalysts.

2. The wide-pore and high-surface area aluminas are the best materials for alumina-catalyzed epoxidation with aqueous H_2O_2 70 wt% [17,18].

3. Concerning the acidic properties of calcined aluminas, the change in H_2O-to-Al molar ratios in sol-gel synthesis provides an useful way to demonstrate that the weak to moderate acid sites are responsible for epoxidation and that the strong acid sites are responsible for H_2O_2 decomposition.

4. The combination of results from ^{27}Al MAS NMR spectra and TPD-NH_3 profiles of calcined aluminas A450-1 to

A450-24 allowed assigning the type Ia Al–OH sites as the catalytic centers for epoxidation. The type Ib Al–OH sites have no activity in catalytic epoxidation with transition aluminas, because ethyl acetate poisons these sites. The strong acid sites of types IIa, IIb, and III Al–OH groups are responsible for the undesirable decrease in selectivity for the oxidant due to H_2O_2 decomposition.

5. The fast drying of the gel is an efficient way to maximize the weak to moderate acid sites on the alumina surface, resulting in higher epoxide yields and higher H_2O_2 efficiencies [17].

6. The role of oxalic acid in the sol-gel synthesis [16,18] is now understood in the same way as the effect of the change in the H_2O-to-Al molar ratio. The presence of oxalic acid acts as a moderator of hydrolysis and polycondensation reactions of the molecular precursors in sol-gel synthesis [3,4], creating the framework of aluminum (oxy-)hydroxides as the oxalate anions coordinate to Al(III) ions, thus changing the hydrolysis and polycondensation rates and providing a higher amount of weak to moderate acid sites that are related to a higher population of terminal hydroxyls (type Ia and Ib) on the alumina surface, which improves the catalytic activity of aluminas.

7. These results also allow us to understand why all of our attempts to synthesize active transition-metal-doped alumina, which takes advantage of both the alumina properties and the enhanced catalytic activity of transition metals, such as tungsten, molybdenum, and titanium, always gave less efficient materials for epoxidation with H_2O_2. Mixed oxides based on alumina and transition metals are typically more acidic than alumina itself [31,32]. Therefore, these materials are shown to be good only for H_2O_2 decomposition, even with transition metal loads of <1 mol%, which should give single-site transition metal oxides.

Supplementary material

XRD patterns and isotherms of nitrogen adsorption–desorption of the calcined aluminas A450-1 to A450-24 at 77 K. Please visit DOI: 10.1016/j.cat.2006.08.024.

References

[1] J. Thornton, Pure Appl. Chem. 73 (2001) 1231.

[2] T.E. Graedel, Pure Appl. Chem. 73 (2001) 1243.

[3] D.K. Ward, E.I. Ko, Ind. Eng. Chem. Res. 34 (1995) 421.

[4] U. Schubert, N. Hüsing, Synthesis of Inorganic Materials, Wiley–VCH, Weinheim, 2000, p. 205.

[5] F. Dumeignil, K. Sato, M. Imamura, N. Matsubayashi, E. Payen, H. Shimada, Appl. Catal. A Gen. 287 (2005) 135.

[6] M. Trueba, S.P. Trasatti, Eur. J. Inorg. Chem. (2005) 3393.

[7] H. Grabowska, L. Syper, M. Zawadzki, Appl. Catal. A Gen. 277 (2004) 91.

[8] Y. Kim, C. Kim, J. Yi, Mater. Res. Bull. 39 (2004) 2103.

[9] J.S. Valente, X. Bokhimi, F. Hernandez, Langmuir 19 (2003) 3583.

[10] J.A. Wang, X. Bokhimi, O. Novaro, T. Lopez, F. Tzompantzi, R. Gomez, J. Navarrete, M.E. Llanos, E.L. Salinas, J. Mol. Catal. A Chem. 137 (1999) 239.

[11] F. Dumeignil, K. Sato, M. Imamura, N. Matsubayashi, E. Payen, H. Shimada, Appl. Catal. A Gen. 241 (2003) 319.

[12] M.C.A. van Vliet, D. Mandelli, I.W.C.E. Arends, U. Schuchardt, R.A. Sheldon, Green Chem. 3 (2001) 243.

[13] J.M.S. Silva, F.S. Vinhado, D. Mandelli, U. Schuchardt, R. Rinaldi, J. Mol. Catal. A Chem. 252 (2006) 186.

[14] D. Mandelli, M.C.A. van Vliet, R.A. Sheldon, U. Schuchardt, Appl. Catal. A Gen. 219 (2001) 2001.

[15] I.W.C.E. Arends, R.A. Sheldon, Top. Catal. 19 (2002) 133.

[16] R.G. Cesquini, J.M.S. Silva, C.B. Woitiski, D. Mandelli, R. Rinaldi, U. Schuchardt, Adv. Synth. Catal. 344 (2002) 911.

[17] R. Rinaldi, U. Schuchardt, J. Catal. 236 (2005) 335.

[18] R. Rinaldi, U. Schuchardt, J. Catal. 227 (2004) 109.

[19] Y. Amenomiya, Y. Morikawa, G. Pleizier, J. Catal. 46 (1977) 431.

[20] J.B. Peri, J. Phys. Chem. 79 (1975) 1582.

[21] R. Rinaldi, J. Sepulveda, U. Schuchardt, Adv. Synth. Catal. 346 (2004) 281.

[22] J. Rebek, R. McCready, Tetrahedron Lett. 45 (1979) 4337.

[23] M. Digne, P. Sautet, P. Raybaud, P. Euzen, H. Toulhoat, J. Catal. 226 (2004) 54.

[24] H. Knözinger, P. Ratnasamy, Catal. Rev.-Sci. Eng. 17 (1978) 31.

[25] T. Hiemstra, W.H. Vanriemsdijk, G.H. Bolt, J. Colloid Interface Sci. 133 (1989) 91.

[26] J.E. Lefler, D.W. Miller, J. Am. Chem. Soc. 99 (1977) 480.

[27] M.J. Duer, Introduction to Solid-State NMR Spectroscopy, Blackwell Publishing, Oxford, 2004, p. 235.

[28] U.G. Nielsen, J. Skibsted, H.J. Jakobsen, Chem. Commun. (2001) 2690.

[29] G.S. Walker, D.R. Pyke, C.R. Werrett, E. Williams, A.K. Bhattacharya, Appl. Surf. Sci. 147 (1999) 228.

[30] S. Bhatia, J. Beltramini, D.D. Do, Catal. Today 7 (1990) 309.

[31] K. Tanabe, Solid Acids and Bases and Their Catalytic Properties, Academic Press, New York, 1970.

[32] K. Tanabe, M. Misono, Y. Ono, H. Hattori, New Solid Acids and Bases and Their Catalytic Properties, Elsevier, Amsterdam, 1989.

[33] J.A. Wang, X. Bokhimi, A. Morales, O. Novaro, T. López, R. Gómez, J. Phys. Chem. B 103 (1999) 299.

[34] D.V. Deubel, G. Frenking, P. Gisdakis, W.A. Herrmann, N. Rösch, J. Sundermeyer, Acc. Chem. Res. 37 (2004) 645.

[35] F.A. Cotton, G. Wilkinson, C. Murillo, M. Bochmann, Advanced Inorganic Chemistry, sixth ed., Wiley, New York, 1999, p. 1303.

[36] V. Vacque, B. Sombret, J.P. Huvenne, P. Legrand, S. Suc, Spectrochim. Acta Part A 53 (1997) 55.

[37] R. Rinaldi, U. Schuchardt, unpublished results.

[38] C.C. Landry, N. Pappe, M.R. Mason, A.W. Apblett, A.N. Tyler, A.N. MacInnes, A.R. Barron, J. Mater. Chem. 5 (1995) 331.

[39] G.W. Kabalka, R.M. Pagni, Tetrahedron 53 (1997) 7999.

[40] R. Buffon, U. Schuchardt, J. Braz. Chem. Soc. 14 (2003) 347.